

Transport and mixing in kinematic and dynamically-consistent flows

P.H. Haynes, D.A. Poet and E.F. Shuckburgh
Department of Applied Mathematics and Theoretical Physics
University of Cambridge.

June 19, 2006

Abstract

The interplay between dynamics and transport in two-dimensional flows is examined by comparing the transport and mixing in a kinematic flow, in which the velocity field is imposed as a given function of time, with that in an analogous dynamically consistent flow in which the advected vorticity field controls the flow evolution. In both cases the variation of the transport and mixing behaviour with a parameter ϵ governing the strength of the time dependence is considered. It is shown that dynamical consistency has the effect of (i) postponing the breaking of a central transport barrier as ϵ increases and (ii) removing the property of the kinematic flow that, for a large range of ϵ , a weakly permeable central barrier persists. (i) is associated with the development of a strong vorticity gradient and associated jet along the central transport barrier. (ii) is associated with the fact that, in the dynamically consistent flow, the breaking of the central barrier is accompanied by a drastic change in the vorticity field and hence in the structure of the flow.

The relation between the vorticity field and transport barriers is further examined using a range of simple kinematic and dynamically consistent models. Implications for formulation of predictive models that represent the interactions between dynamics and transport and mixing are discussed.

1 Introduction

The transport and mixing properties of atmospheric and oceanic flows have been extensively studied over the last ten years or so (e.g. Pierrehumbert and Yang 1993, Koh and Plumb 2000, Joseph and Legras 2002, Wiggins 2005), motivated by the need for better understanding of the transport and mixing of chemical and biological tracers. Progress has been aided by improved numerical simulations and by the rapid growth of observational data on chemical and biological species. Study of transport and mixing is also relevant to the underlying dynamics of large-scale atmospheric and oceanic flows, since the dynamical equations can be expressed to good approximation as the conservation of potential vorticity (PV) following the fluid motion (with non-conservation associated with frictional or diabatic effects), together with an invertibility relation that determines all other flow quantities instantaneously from the potential vorticity (e.g. Hoskins et al 1985).

Atmospheric and oceanic studies have benefitted significantly from the study of transport and mixing from the mathematical point of view, through the development of chaotic advection as an application of dynamical systems theory (e.g. Wiggins 1992). By chaotic advection we mean the phenomenon that, in a velocity field that is a relatively simple function of space and time, particle paths can be chaotic, i.e. sensitive to initial conditions so that particles that are initially close together rapidly separate and hence to complex patterns of particles or of an advected tracer.

Many aspects of chaotic advection have been explored in so-called kinematic models in which the velocity field is imposed as a given function of space and time and the resulting transport and mixing properties of the flow are calculated, e.g. by following fluid particles. The flows considered are often taken to be time-periodic, in which case the advection problem reduces to the repeated application of a map. An ubiquitous feature of such flows (or the corresponding maps) is that the transport and mixing structure is highly inhomogeneous with chaotic regions, within which there is rapid separation of nearby particles and hence effective mixing, coexisting with and separated by barrier regions, across which there is no transport and within which particle separation is slow (e.g. see Meiss 1992).

A characteristic feature of many observed flows in the atmosphere and in the ocean and many numerical simulations of analogous flows is similar inhomogeneous transport and

mixing behaviour, with regions of strong mixing separated by transport barriers. Examples include the stratospheric polar night jet (e.g. Juckes and McIntyre 1987, Norton 1994, Waugh and Plumb 1994, Chen 1994) which acts as a barrier with mixing regions inside, in the polar vortex interior, and outside, in the so-called stratospheric surf zone, the subtropical jet (e.g. Chen 1995, Haynes and Shuckburgh 2000), with adjoining mixing regions in the tropical upper troposphere and in the mid- and high- latitude polar stratosphere and the Gulf Stream and similar oceanic current systems (e.g. Bower et al 1985, Marshall et al 2006).

The significance of the similarity between the inhomogeneous transport and mixing structure seen in the kinematic time-periodic flows on the one hand and in observed or realistic atmospheric and oceanic flows on the other is not yet completely clear. The fact is that in the former the flow is imposed in advance whilst in the latter the flow is the self-consistent solution of a set of dynamical equations. Indeed, for flows where the dynamics are governed by material conservation of PV, it might be argued that if particle trajectories are chaotic, the PV field will naturally assume a spatially complex, time varying configuration and applying an inversion operator to this flow will almost always not give the flow field that has been assumed, resulting in what might be described as a ‘dynamical consistency’ problem. Brown and Samelson (1994) argue in the case of two-dimensional PV conserving flow that one implication of dynamical consistency is that chaotic particle trajectories are in fact forbidden, though it may be possible to escape this constraint if PV is not perfectly conserved. One argument for the relevance of the kinematic models is that the potential vorticity field arising from the transport and stirring is in many cases dominated by small spatial scales and the smoothing nature of the inversion operator is such that the dynamical effect is weak. However it is difficult to see that the dynamical effect will always be weak and it seems likely that in some aspects of transport and mixing behaviour, e.g. the persistence versus destruction of transport barriers as perturbation amplitude is increased, the dynamical effect will be significant. It seems extremely difficult to formulate any analytic or semi-analytic model that allows an interesting combination of dynamical consistency and chaotic transport. One approach to addressing the dynamical consistency problem has been to choose special flows in which advection of potential vorticity for some reason has no implications for the dynamics. (del-Castillo-Negrete and Morrison 1993, Ngan and Shepherd 1997). Unfortunately these special flows can almost by definition give no insight into flows for which mixing and transport interacts in a non-trivial way with

dynamics.

Thus an important question is how the predictions of kinematic chaotic advection studies carry over to the 'dynamically consistent' case, where potential vorticity is materially conserved and as it evolves in time, determines the flow through inversion. A refinement of this question is whether there are robust guiding principles that can be used to gain an understanding of such flows, in numerical simulation or a naturally occurring flow.

Given that any interesting interaction between chaotic mixing and transport and dynamics is by nature complex and unlikely to yield to any systematic approximation procedure, the approach that we take in this paper is to report results from a combination of kinematic studies and numerical simulations and attempt to draw general conclusions from these. All these studies are based on 2-dimensional flows or maps in the (x, y) plane. Bearing in mind atmospheric applications we regard x as a longitudinal coordinate and y as a latitudinal coordinate.

Firstly in Section 2 we note that in kinematic studies in which a sequence of flows is considered which transport becomes increasingly more chaotic it is almost always the case that the last barrier to break coincides with the axis of a jet.

Secondly in Section 3 we carefully compare a typical kinematic problem and a corresponding dynamically consistent problem. We show through numerical simulation that dynamical consistency raises the threshold level of perturbation required to break a transport barrier. In this sense dynamical consistency strengthens transport barriers. However we also show that once the threshold amplitude for a strong barrier to be broken is past, then the breaking of the barrier in the dynamically consistent case is much more catastrophic than in the kinematic case.

Finally in Section 4 we consider the well-known self-organising property of forced two-dimensional turbulent flow on a β -plane into persistent jets. Such self-organisation might be thought of as resulting from the fact that where potential vorticity gradients are strong mixing is inhibited and where they are weak mixing is favoured. One aspect of this is that strong gradients in potential vorticity inhibit lateral displacement of fluid parcels through the Rossby restoration mechanism, in loose analogy with the inhibition of vertical displacements of fluid parcels by strong buoyancy gradients. A second aspect is that sharp gradients of potential vorticity are inevitably associated with jets (which in Section 2 we have noted tend to act naturally as barriers in kinematic studies).

By comparing transport of tracer under the full velocity field, and under a modified

velocity field from which the longitudinal mean has been removed, we show that the second aspect above is an essential part of the transport barrier mechanism in these flows. Thus any attempt to derive a simple parametrisation of transport as a function of potential vorticity gradient needs to take this into account.

2 Kinematic studies of jets

A traditional approach in kinematic studies has been to follow particle advection in a time-periodic flow. One simplifying feature of time-periodic flows is that the advection problem can be reduced to considering a map that represents the action of advection over one time period of the flow.

In this paper we are primarily concerned with the issue of transport barriers and how they change as the parameters of the flow change. One much studied map is the so-called 'standard map' defined on the unit square, extended periodically in both directions, which is the product of a shear in the x -direction and displacement in the y direction with sinusoidal dependence on x . In this system it is natural to consider the changes in transport that occur as the amplitude of the sinusoidal displacement increases. For zero amplitude the particles are mapped in the x -direction and each line $y = \text{constant}$ is a barrier to transport in the y -direction. When the amplitude is non-zero but small there are still barriers to transport in the y direction, i.e. unbounded particle displacements in the y direction are not possible. At a critical value of amplitude the last barrier breaks and for larger amplitudes particle displacements in the y direction may be unbounded. There has been a great deal of mathematical study of the breaking of the last barrier, which hinges on number-theoretic properties of the 'frequency' of each barrier (i.e. the average rate of crossing the unit square along that barrier) (e.g. Meiss 1992). But it is not clear that this tells us anything useful about transport properties of most atmospheric and oceanic flows, not least because the standard map (and hence any underlying flow that it represents) has non-vanishing shear.

In any flow containing a jet, and hence in any map that might be used to represent the advection properties of that flow, the shear changes sign at the axis of jet. Therefore insights gained from the standard map may not be at all relevant.

del-Castillo-Negrete and Morrison (1993), del-Castillo-Negrete (2000), Yang (2000) and others have examined the transport properties of jet-like flows, both using continuous-time

time-periodic flows and also using suitably defined maps (which del-Castillo-Negrete and Morrison call the ‘standard non-twist map’) (see also del-Castillo-Negrete et al, 1996). They use various heuristic methods well known in dynamical systems theory to give a simple theoretical description of the behaviour. One of these is the so-called ‘resonance’ overlap criterion that for two superposed waves of different phase speeds considers the cat’s eye streamlines surrounding the critical lines of the two waves and predicts chaos when the two sets of cat’s eyes intersect. This might suggest that whether or not the jet axis is the last barrier depends crucially on the phase speeds of the disturbances relative to the flow speed at the jet axis. A similar argument has been used by Bowman (1993a,b) to argue that the effectiveness of the stratospheric jet as a barrier to transport depends on the fact that the phase speeds of the wave disturbances do not match the jet speed. Here we simply emphasise the point that the ‘last barrier’ seems invariably to correspond to the axis of the jet, whatever the relation between the flow speed at the jet maximum and the phase speeds of the wave disturbances.

We will consider the following map:

$$x_{n+1} = x_n + \exp[(y - \pi)^2] + 0.65(y - \pi) + C \quad (1)$$

$$y_{n+1} = y_n + \epsilon x_n, \quad (2)$$

where C is a constant. This is somewhat different to that considered by del-Castillo-Negrete and Morrison (1993), but is a member of family of maps that allows investigation of the effect of changing the location where the shear is zero and also changing the absolute value of the velocity at the zero-shear location. The map is defined on a domain that is unbounded in y and 2π -periodic in x . We focus on the behaviour in $0 < y < 2\pi$, shown in Figure 1. For the map above the shear is independent of the constant C , and for all C there are two values of y in $0 < y < 2\pi$ for which the shear vanishes.

As noted by del-Castillo-Negrete and Morrison (1993), the continuous time flow corresponding to such a map is one where the x -dependent part of the flow varies in time as a repeating delta function. The corresponding Fourier series in time has coefficients that are independent of frequency, i.e. the x -dependent part of the flow may be regarded as an infinite superposition of waves, with uniform separation in phase speed between each wave, and with each wave having the same amplitude.

Analogous to the other maps and flows discussed above, there is a regime for small ϵ where large particle displacements in the y -direction, specifically from $y = 0$ to $y = 2\pi$,

are forbidden by the presence of barriers. The threshold value of ϵ at which the last barrier breaks depends on the constant C . The cases shown in Figure 1 are all for values of ϵ slightly lower than the threshold value. The important point here is that the location of the 'last barrier' does not seem to depend on the value of C , as it might do if the phase speeds of the disturbing waves were crucial.

3 Comparison between kinematic and dynamically consistent models

A much studied kinematic model is flow in a channel comprising two waves propagating with different frequencies. This has variously been presented as a model for Rayleigh-Benard convection (Weiss and Knobloch 1989) and as a model for Rossby waves (Pierrehumbert 1991). In the rest frame of one of the waves the flow might be described as a meandering jet with an imposed time-periodic perturbation. The amplitude of the time-periodic perturbation may be represented by the parameter ϵ . When $\epsilon = 0$ the flow is steady and particles move along streamlines. For ϵ greater than zero there are thin chaotic regions, separated by barriers, and as ϵ is increased these chaotic regions enlarge and merge, but with at least one barrier region remaining to prevent transport across the channel. An important transition takes place when ϵ reaches a critical value at which the last barrier to transport across the channel breaks and the topology of the barriers and mixing regions changes. For larger values of ϵ there may be barriers, but there is no barrier that divides upper and lower or northern and southern regions of the channel. This behaviour has been described by several previous authors. Pierrehumbert (1991) has gone further by considering a similar dynamically consistent model, but in this paper he tends to focus on the morphology of the mixing (the role of heteroclinic points etc) rather than the 'last barrier' transition.

Here we compare a particular kinematic model, in which the flow is given by the streamfunction

$$\psi(x, y, t) = -0.5y + \sin x \sin y + \epsilon \sin(x - 0.3t) \sin 2y, \quad (3)$$

representing a time-periodic flow with period $2\pi/0.3$, with a corresponding dynamical model, based on the two-dimensional equations on a β -plane with topographic forcing

$$\frac{\partial}{\partial t} \nabla^2 \tilde{\psi} + 0.5 \frac{\partial}{\partial x} \nabla^2 \tilde{\psi} + J(\tilde{\psi}, \nabla^2 \psi) + 0.5 \frac{\partial}{\partial x} \tilde{\psi} = -h_t - 0.5h_x, \quad (4)$$

where the total streamfunction $\psi = -0.5y + \tilde{\psi}$ and β has been taken to be 0.5. The topographic forcing $h(x, y, t)$ is given by

$$h(x, y, t) = \sin x \sin y + 2.5\epsilon \sin(x - 0.3t) \sin 2y \quad (5)$$

The flow is taken to be 2π -periodic in the x -direction and to lie between rigid boundaries at $y = 0$ and $y = \pi$. Note that the particular values of the constants in (4) are chosen for illustrative processes. Extensive investigation has shown the sort of behaviour reported below does not depend on the particular choices for those constants.

The two models are comparable in the sense that if the wave amplitudes are small and the initial $\tilde{\psi}$ is chosen to match (3) at $t = 0$, then the flow in each will be the same. For finite wave amplitudes what happens in practice is that (for non-zero ϵ) the flow evolves during the first few time periods to a different quasi-periodic state from (3). An example is shown in Fig. 2 for $\epsilon = 0.05$. In this case, since ϵ is small, the quasi-periodic state attained after the initial adjustment period is only very slightly different from that implied by the initial condition. In the description of transport and mixing properties later, all diagnostics are applied in the quasi-periodic regime after the initial adjustment.

The transport and mixing properties of the kinematic model described have already been much studied, e.g. in the papers previously cited. For the particular choice of parameters above, the critical value of ϵ at which the the last central barrier breaks is about 0.34.

Several different methods have been used previously to identify and quantify barriers in this sort of kinematic model, see for example Shuckburgh and Haynes (2003). Here we show results from a particle-based method in which particles are released in a region on one side of the central barrier (the ‘source’ region) and the time for them to reach a second region on the other side of the central barrier (the ‘receptor’ region) is calculated. Poet (2004) has shown carefully that this method is robust in the sense that the calculated time to cross the barrier is insensitive to the precise choice of ‘source’ and ‘receptor’ regions. Applying this method to the kinematic problem for different values of ϵ gives the results shown in Figure 3, which depicts the time for crossing the central barrier as a function of ϵ , shown by the blue graph. The time is essentially infinite for $\epsilon < 0.34$ and for $\epsilon > 0.34$ is a slowly decreasing function of ϵ . The slowness of the decrease for $\epsilon > 0.34$ may result from the existence of ‘cantori’ – partial barriers that are left when the last absolute barrier breaks – or from the stickiness of smaller barrier regions that are left

once the main central barrier has broken (e.g. Meiss 1992), but the precise explanation is not particularly important for the present discussion.

A first question is whether there is an analogue of the central barrier for the dynamically consistent problem. The red graph in Figure 3 shows the corresponding time to cross the central barrier in the dynamically consistent problem, again as a function of ϵ . There are some important differences between the behaviour for the dynamically consistent problem and that for the kinematic problem. The value of the crossing time is generally smaller for a given value of ϵ for the dynamically consistent model versus the kinematic model. However in the dynamically consistent case the precise flow that is realised depends, for example, on the initial conditions, and it is difficult to set up conditions where any transport barrier is perfect. The relatively large, but not infinite, values of the crossing time for $\epsilon < 0.44$ in the dynamically consistent case are therefore interpreted as implying the presence of a strong central barrier which breaks at $\epsilon \simeq 0.44$. Under this interpretation the dynamical consistency has strengthened the central barrier, allowing it to persist to $\epsilon \simeq 0.44$ rather than $\epsilon \simeq 0.34$. A further striking difference is that for $\epsilon > 0.44$ the crossing time drops abruptly to small values, rather than decreasing slowly. This behaviour will be explained below.

It is interesting to consider the PV field that results for different values of ϵ . Fig. 4 shows the PV field in the quasi-periodic stage of the evolution for different values of ϵ , including one value for which the central barrier has broken. For values of ϵ where the central barrier persists, there are significant spatial variations in the value of the PV. As ϵ increases, the PV field on each side of the barrier become more homogeneous, consistent with the picture obtained from kinematic investigations that individual chaotic regions on one side of the central barrier tend to merge as ϵ increases. Thus, for $\epsilon = 0.4$, just less than the threshold required for the central barrier to break, the PV field is essentially homogeneous on either side of the barrier. The crucial difference between kinematic and dynamically consistent models seems to arise as ϵ increases through the threshold value for the barrier to break. In the kinematic case the velocity field, and hence the transport and mixing properties, are a continuous function of ϵ . In the dynamically consistent case on the other hand, the PV homogenises across the whole domain as the central barrier breaks. The time evolution of this process is shown in Fig. 5 for $\epsilon = 0.5$. (Contrast the time evolution shown in Fig. 5 for $\epsilon = 0.05$.) The result is that the flow, and therefore the transport and mixing properties, change almost discontinuously as a function of ϵ .

The assumption of homogenisation of the PV implies that

$$\nabla^2\psi + \beta y + h(x, y, t) = \beta\pi/2 \quad (6)$$

where the constant on the right-hand side is determined by the average PV set by the initial condition. Recall that in the simulations shown here β is taken to be 0.5. Given the time-periodic topographic forcing defined by (5), this defines a new kinematic problem in which the flow is time periodic and given by the solution of (6) subject to the boundary conditions. Analysis of the transport and mixing properties in this new kinematic problem show that a very large proportion of the domain is filled by a single chaotic mixing region, with one or two very small regions isolated by transport barriers. This is shown explicitly by the Poincaré section for this new kinematic problem shown in Fig. 6. The homogenisation assumption is therefore self-consistent to good approximation.

The conclusion is therefore that the dynamically consistent flow does not show an extended partial barrier regime characteristic of the kinematic case because once the central barrier is broken the PV is stirred throughout the flow domain and the character of the flow changes drastically as a result.

4 Transport and mixing in 2-D β -plane turbulence

We now move on to consider some aspects of transport and mixing behaviour in forced-dissipative 2-D β -plane turbulence. It is well known that homogeneous isotropic small-scale random forcing on a doubly periodic domain gives rise to an upscale energy cascade and to the formation of persistent narrow eastward longitudinal jets, whose separation is roughly $(U/\beta)^{1/2}$, where U is a typical velocity (at the scale of the jets). (Rhines 1975, Vallis and Maltrud 1993, Maltrud and Vallis 1991, Danilov and Gurarie 2004.) The eastward jets are associated with strong gradients of potential vorticity. The regions between the jets tend to have relatively weak gradients of potential vorticity (e.g. Danilov and Gurarie 2004, Figure 1).

An attractive explanation/description of the formation of these jets is based on the transport and mixing of potential vorticity, if it is accepted that potential vorticity gradients tend to inhibit mixing. If some small-amplitude modulation is applied to a system where large-scale PV gradients are uniform, then where the gradients are relatively weak the mixing is expected to be relatively strong and where the gradients are relatively strong the

mixing is expected to be relatively weak. The effect will be to reduce gradients where they are relatively weak and, since strong gradient regions sit between weak gradient regions, to enhance gradients where they are relatively strong. Thus one might naturally realise a state where there are large-amplitude variations in potential vorticity gradient, with a limiting form where the flow is partitioned into regions within which potential vorticity is almost constant, separated by narrow regions where the potential vorticity gradient is very large. The corresponding flow, by PV inversion, naturally has narrow eastward jets centred on the sharp gradient regions. (See Dritschel and McIntyre, 2006, for further discussion).

There is a useful analogy between the idea that horizontal mixing of PV is inhibited by strong horizontal gradients of PV and the idea, applying to density stratified fluids, that vertical mixing is inhibited by strong vertical gradients of density. The formation of constant density layers in stratified fluids in which turbulence is driven by some kind of stirring (Phillips 1972) has been explained by something like the argument given in the preceding paragraph. Explicit mathematical models have been devised to give a firmer quantitative basis for this mechanism (Phillips 1972, Posmeinter 1977, Balmforth et al 1998) Take the Balmforth et al model as an example. Along with other models it represents density transport through a diffusive turbulent eddy flux and therefore requires prediction of eddy diffusivity, which is taken to be the product of the turbulent kinetic energy density and a mixing length, the latter depending on the forcing length scale, the kinetic energy and the buoyancy gradient. The important point here is that the formation of the density structure occurs because the turbulent eddy diffusivity is small where the buoyancy gradient is large and large where the buoyancy gradient is small.

Could a similar model be formulated to describe the formation of β -plane jets?

We consider transport and mixing in a simulation that is typical of many that have been reported in the literature. The relevant equations are

$$\frac{\partial}{\partial t} \nabla^2 \psi + J(\psi, \nabla^2 \psi) + \beta \frac{\tilde{\partial}}{\partial x} \psi = F(x, y, t) - \alpha \nabla^2 \psi + \kappa \nabla^6 \psi. \quad (7)$$

The terms on the right-hand side represent, respectively, forcing (taken to be a stochastic function of time), linear damping and fourth-order hyperdiffusion. The forcing term is prescribed in the same way as several previous investigations, e.g. as described by Smith et al (2002), i.e. $\hat{F}(\mathbf{k}, t + \delta t) = c\hat{F}(\mathbf{k}, t) + (1 - c^2)e^{1/2}e^{i\phi(\mathbf{k})}$, where $\hat{F}(\mathbf{k}, t)$ is the Fourier

transform of $F(x, y, t)$, \mathbf{k} is wavenumber, δt is the model time step. e is a constant that sets the magnitude of the forcing and c is a constant controlling the correlation time for the forcing. $\phi(\mathbf{k})$ is a phase chosen randomly from one time step to the next. If $c = 1 - \tau^{-1}\delta t$ then, for δt small enough, the autocorrelation of the forcing decays exponentially in time at rate τ^{-1} . For reference, in the simulation to be reported, $\beta = 5$, $\alpha = 1$, $\kappa = 10^{-3}$, the forcing is applied for wavenumbers \mathbf{k} such that $44 \leq |\mathbf{k}| \leq 46$ and τ is chosen to be 1. The constant e is chosen such that the equilibrated kinetic energy integrated over the domain is about 0.3. The numerical model is based on a spectral scheme with 256×256 wavenumbers.

This simulation, along with many others, gives rise to a clear set of longitudinal jets, shown in Fig. 7(a) as a colour plot of longitudinal mean longitudinal velocity \bar{u} as a function of y and t . In this case there five distinct jets, one of which might be described as a double jet at the beginning of the simulation and which appears to be narrowing to a single jet as the simulation proceeds.

To quantify the transport and mixing structure in this flow we use the effective diffusivity diagnostic (e.g. Nakamura 1996, Shuckburgh and Haynes 2003) calculated from an advected tracer field. The effective diffusivity, which is small in barrier regions and large in mixing regions, is a function of an equivalent- y coordinate and is shown in Fig. 7(c) as a function of equivalent- y and t . For technical reasons it is most straightforward to calculate the effective diffusivity in a smaller domain that omits regions close to the limits in y of the full domain. This subdomain contains only three of the five jets, one of which is the 'double jet'. The effective diffusivity shows clear minima at the location of the eastward jets, consistent with the notion of the jets as transport barriers. (Note the the 'double jet' is seen as a double transport barrier.)

One might try to explain these barriers, indicated by minima in the effective diffusivity, as minima of a turbulent eddy diffusivity, along the lines of the Balmforth et al (1998) model for density stratified flows. The turbulent eddy diffusivity encodes the transport effect of the longitudinally varying part of the flow. We may consider this transport effect by following the evolution of a second tracer that is advected by a modified flow obtained by removing the longitudinal mean part from the full flow (a similar study has been conducted using velocity fields from the surface Southern Ocean by Marshall et al 2006). The effective diffusivity calculated from this second tracer is shown in Fig. 7(d). This is strikingly different from the effective diffusivity for the first tracer. In the second

case the eastward jets correspond to maxima in the effective diffusivity, not minima (and a similar difference was observed in the Marshall et al 2006 calculations). Part of the explanation for the difference observed here comes from the structure of \bar{v}^2 , where v is the y component of velocity, shown as a function of y and t in Fig. 7(b). It may be seen that the largest amplitudes of \bar{v}^2 tend to be centred on the eastward jets, perhaps because these act as a kind of waveguide for Rossby wave activity. It is therefore not surprising that the most effective transport of the tracer also occurs in regions centred on these jets. Note that the ‘double’ jet appears as a single maximum in the effective diffusivity, but that this is consistent with the lack of clear separation between the two maxima \bar{v}^2 associated with the two parts of this double jet.

The conclusion from the above is that the barrier effect of the jets is not simply a result of the modulation by the jets of the transport properties of the longitudinally varying part of the flow, as would be implicit in any attempt to model those transport properties along the lines proposed by Balmforth et al (1998) for the density stratified problem. The jets themselves must play a direct role in the transport. There is clearly some relation of this to the argument of Jukes and McIntyre (1987, see also Dritschel and McIntyre, this issue), that background shear plays an important role in the the vortex-edge transport barrier, except that, as argued previously in §2, there is evidence that it is the location of zero shear (between shears of opposite sign) that is the preferred location of the barrier. There seems to be little close relation with the ‘shear-shielding’ mechanism described by Hunt and Durbin (1999) which emphasises the role of isolated vortex sheets in which vorticity is strong and single-signed.

5 Summary

In this paper we have considered transport and mixing in PV conserving dynamically consistent flows. We have made no attempt to present any precise theory, in part because all routes to such a theory seem to require some assumption, e.g. scale-separation between eddies and jets, that clearly does not apply to flows of interest. Instead we have presented a set of results from different models, each of which seems to have some relevance.

Our main conclusions are as follows:

- (i) In kinematic models of jet-like flows, with velocity field imposed as a function of space and time, the ‘last’ barrier (last remaining as the amplitude of a perturbation is

increased) invariably corresponds to the axis of a jet. This suggests that whilst shear is an important ingredient of the barrier effect, it is the zero-shear location, between two regions of opposite-signed shear, that is the strongest barrier (rather than any location determined by maximum difference between background flow and phase speed of disturbances, for example).

(ii) Dynamically consistent flows show some common transport and mixing behaviour with corresponding kinematic models, in particular a jet-like flow that is weakly perturbed from steady shows a strong central transport barrier in both cases and this barrier breaks as the perturbation increases beyond a threshold value. However, as illustrated in §3, dynamical consistency significantly increases this threshold value and furthermore the nature of the transport is very different beyond the threshold value.

(iii) The previously mentioned increase in the threshold value for breaking of the barrier is concrete evidence for the role of dynamical consistency in PV conserving flows in enhancing the transport barrier effect. Thus whilst strong gradients of PV in simulated or observed flows may in principle be a passive result of strong stirring regions separated by a barrier region, we have clear evidence that in the flows considered here those strong gradients tend to enhance the effectiveness of the barrier.

(iv) The association of stronger PV gradients with enhanced barriers to transport (and reduced PV gradients with enhanced mixing) gives a natural explanation for the spontaneous appearance of eastward jets in β -plane turbulence. However, this effect is not simply described by a reduced turbulent eddy diffusivity in the regions of strong PV gradient. The eastward jets associated (via PV inversion) with the strong PV gradients play a direct role in the enhanced barrier effect, as suggested by (i). Any attempt to formulate a predictive model of the jet formation would have to incorporate this effect, by combining some representation of the turbulent eddies with the presence of the background flow to give some kind of effective diffusivity.

Acknowledgements: DAP was supported by the UK Natural Environment Research Council through a PhD studentship. The authors have benefitted from useful discussions with M.E.McIntyre, R.S. McKay and W.R. Young. The channel model code on which the work reported in §3 was based was originally provided by P.D. Killworth.

References

- Balmforth, N.J., Llewellyn Smith, S.G., Young, W.R 1998: Dynamics of interfaces and layers in a stratified turbulent fluid. *J. Fluid Mech.*, 355, 329-358.
- Bower, A.S., Rossby, H.T., Lillibridge, J.L, 1985: The Gulf Stream – barrier or blender? *J. Phys. Oceanogr.*, 15, 24-32.
- Bowman, K. P., 1993: Barotropic simulation of large-scale mixing in the Antarctic polar vortex. *J. Atmos. Sci.*, 50, 2901–2914.
- Bowman, K. P., 1993: Large-scale isentropic mixing properties of the Antarctic polar vortex from analyzed winds. *J. Geophys. Res.*, 98, 23013–23027.
- Brown, M.G., Samelson, R.M., 1994: Particle motion in incompressible, inviscid vorticity conserving fluids. *Phys. Fluids*, 6, 2875-2876.
- Chen, P., 1995: Isentropic cross-tropopause mass exchange in the extratropics. *J. Geophys. Res.*, 100, 16661–16673.
- Danilov, S., Gurarie, D., 2004: Scaling, spectra and zonal jets in β -plane turbulence. *Phys. Fluids*, 16, 2592–2603.
- del-Castillo-Negrete, D., 2000: Chaotic transport in zonal flows in analogous geophysical and plasma systems. *Phys. Plasmas*, 7, 1702-1711.
- del-Castillo-Negrete, D., Morrison, P. J., 1993: Chaotic transport by Rossby waves in shear flow. *Phys. Fluids*, A5, 948–965.
- del Castillo-Negrete, D., Greene, J. M., Morrison, P. J., 1996: Area-preserving non-twist maps: periodic orbits and transition to chaos. *Physica D*, 91, 1–23.
- Dritschel, D.G., and McIntyre, M.E., 2006: Multiple jets as PV staircases: the Phillips effect and the resilience of eddy-transport barriers. *J. Atmos. Sci.*, submitted to Savannah meeting special issue.
- Haynes, P. H., Shuckburgh, E. F., 2000: Effective diffusivity as a diagnostic of atmospheric transport. Part I: stratosphere. *J. Geophys. Res.*, 105, 22777-22794
- Haynes, P. H., Shuckburgh, E. F., 2000: Effective diffusivity as a diagnostic of atmospheric transport. Part II: troposphere and lower stratosphere. *J. Geophys. Res.*, 105, 22795-22810.
- Hunt, J. C. R., Durbin, P. A., 1999: Perturbed vortical layers and shear sheltering. *Fluid Dyn. Res.*, 24, 375–404.

- Joseph, B., Legras, B. 2002: Relation between kinematic boundaries, stirring and barriers for the Antarctic polar vortex. *J. Atmos. Sci.*, 59, 1198–1212.
- Juckes, M. N., McIntyre, M. E., 1987: A high resolution, one-layer model of breaking planetary waves in the stratosphere. *Nature*, 328, 590–596.
- Koh, T.-Y., Plumb, R.A., 2000: Lobe dynamics applied to barotropic Rossby-wave breaking. *Phys. Fluids* 12, pp.1518-1528.
- Marshall, J., Shuckburgh, E., Jones, H., Hill, C., 2006: Estimates and implications of surface eddy diffusivity in the southern ocean derived from tracer transport. *J. Phys. Oceanogr.*, 36, (to appear).
- Maltrud, M. E., Vallis, G. K., 1991: Energy spectra and coherent structures in forced two-dimensional and beta-plane turbulence. *J. Fluid Mech.*, 228, 321–342.
- Meiss, J. D., 1992: Symplectic maps, variational principles and transport. *Rev. Mod. Phys.*, 64, 795–848.
- Nakamura, N., 1996: Two-dimensional mixing, edge formation, and permeability diagnosed in area coordinates. *J. Atmos. Sci.*, 53, 1524–1537.
- Ngan, K., Shepherd, T. G., 1997: Chaotic mixing and transport in Rossby-wave critical layers. *J. Fluid Mech.*, 334, 315–351.
- Norton, W. A., 1994: Breaking Rossby waves in a model stratosphere diagnosed by a vortex-following coordinate system and a technique for advecting material contours. *J. Atmos. Sci.*, 51, 654–673.
- Ottino, J. M., Leong, C. W., Rising, H., Swanson, P. D., 1986: Morphological structures produced by mixing in chaotic flows. *Nature*, 333, 419–425.
- Phillips, O.M., 1972: Turbulence in a strongly stratified fluid – is it unstable? *Deep-Sea Res.*, 19, 79-81.
- Pierrehumbert, R. T., 1991: Chaotic mixing of tracer and vorticity by modulated traveling Rossby waves. *Geophys. Astrophys. Fluid Dyn.*, 58, 285–319.
- Pierrehumbert, R. T., Yang, H., 1993: Global chaotic mixing on isentropic surfaces. *J Atmos Sci*, 50, 2462–2480.
- Poet, D.A., 2004: Dynamical consistency, barriers to transport and mixing, in chaotic advection flows. Ph.D. thesis, University of Cambridge, pp.207, 2004.

- Posmeinter, E.S., 1977: The generation of salinity finestructure by vertical diffusion. *J. Phys. Oceanogr.*, 7, 298-300.
- Rhines, P. B., 1975: Waves and turbulence on a beta-plane. *J. Fluid Mech.*, 69, 417-443.
- Smith, K.S., Boccaletti, G., Henning, C.C., Marinov I., Tam C.Y., Held I.M., Vallis, G.K. 2002: Turbulent diffusion in the geostrophic inverse cascade. *J. Fluid Mech.*, 469, 13-48.
- Shuckburgh, E. F., Haynes, P. H., 2003: Diagnosing transport and mixing using a tracer-based coordinate system, *Phys. Fluids*, 15, 3342-3357.
- Vallis, G. K., Maltrud, M. E., 1993: Generation of mean flows on a beta plane and over topography. *J. Phys. Oceanogr.*, 23, 1346-1362.
- Waugh, D. W., Plumb, R. A., 1994: Contour advection with surgery: a technique for investigating finescale structure in tracer transport. *J. Atmos. Sci.*, 51, 530-540.
- Weiss, J. B., Knobloch, E., 1989: Mass transport by modulated travelling waves. *Phys. Rev. A*, 40, 2579-2589.
- Wiggins, S., 1992: *Chaotic transport in dynamical systems*. New York, Springer-Verlag, 301pp.
- Wiggins, S., 2005: The dynamical systems approach to lagrangian transport in oceanic flows. *Ann. Rev. Fluid Mech.*, 37, 295-328.
- Yang, H., 1998: The central barrier, asymmetry and random phase in chaotic transport and mixing by Rossby waves in a jet. *Int. J. Bifurcation and Chaos*, 8, 1131-1152.

List of Figures

Figure 1: (b), (d) and (f) show Poincaré sections for the map defined by (1) and (2). A small number of points in the (x, y) plane are used as initial conditions for the map and successive iterations are plotted. In chaotic regions the iterates of the map fill out a region of finite area. In barrier regions the iterates of the map fill out a curve. In each case the value of ϵ is chosen to be close to, but less than, the threshold for the 'last barrier' (to transport in the y direction) to disappear. Values of (C, ϵ) are (b) $(0, 1.5)$, (d) $(1, 1.75)$, (f) $(2, 0.5)$. (a), (c), (e) show the corresponding longitudinal displacement (blue) and longitudinal shear (red) profiles. In each of cases (b), (d) and (f) the remaining barrier region is clear as the region where the density of points is low. A rough correspondence is clear between the zero shear locations in (a), (c) and (e) and the remaining barrier regions in (b), (d) and (f). The correspondence is made precise by assigning a longitudinal velocity – defined by the average rate that iterates of the map move in the x -direction – to each of the curves that is mapped out in (b), (d) or (f) (or corresponding curves that could be mapped by starting with different initial conditions). Once a longitudinal velocity has been assigned then it is straightforward to determine the longitudinal shear.

Figure 2: PV field for the case $\epsilon = 0.05$ at times (a) $t = 0$, (b) $t = 0.5\pi/0.3$, (c) $t = \pi/0.3$, (d) $t = 16\pi/0.3$. Note that $2\pi/0.3$ is the period of the imposed topographic forcing in 5. The black and white curves highlight PV contours chosen to coincide with the heteroclinic streamlines (those joining stagnation points) in the initial flow.

Figure 3: Average transit times to cross the central transport barrier as a function of ϵ in the kinematic model (blue) and the dynamically consistent model (red). See text for discussion.

Figure 4: PV field at times $t = 200\pi/0.3$ ($2\pi/0.3$ is the period of the imposed topographic forcing in 5) for (a) $\epsilon = 0$, (b) $\epsilon = 0.05$, (c) $\epsilon = 0.1$, (d) $\epsilon = 0.3$, (e) $\epsilon = 0.4$, (f) $\epsilon = 0.5$. Note that for $\epsilon = 0.5$ the central barrier breaks and the PV therefore essentially homogenises over the domain.

Figure 5: PV field for the case $\epsilon = 0.5$ at times (a) $t = 0$, (b) $t = 2\pi/0.3$, (b) $t = 4\pi/0.3$, (c) $t = 8\pi/0.3$, (b) $t = 16\pi/0.3$, (b) $t = 20\pi/0.3$. Note that $2\pi/0.3$ is the period of the imposed forcing in 5.

Figure 6: Poincaré section arising from the flow defined by (6) and (5), generated by

three initial conditions, two of which lie on barriers and third of which maps out the large chaotic mixing region that covers most of the domain.

Figure 7: (a) \bar{u} as function of y and t , (b) $\overline{v^2}$ as function of y and t , (c) κ_{eff} calculated from tracer advected with full velocity field, (d) κ_{eff} calculated from tracer advected with \bar{u} removed.

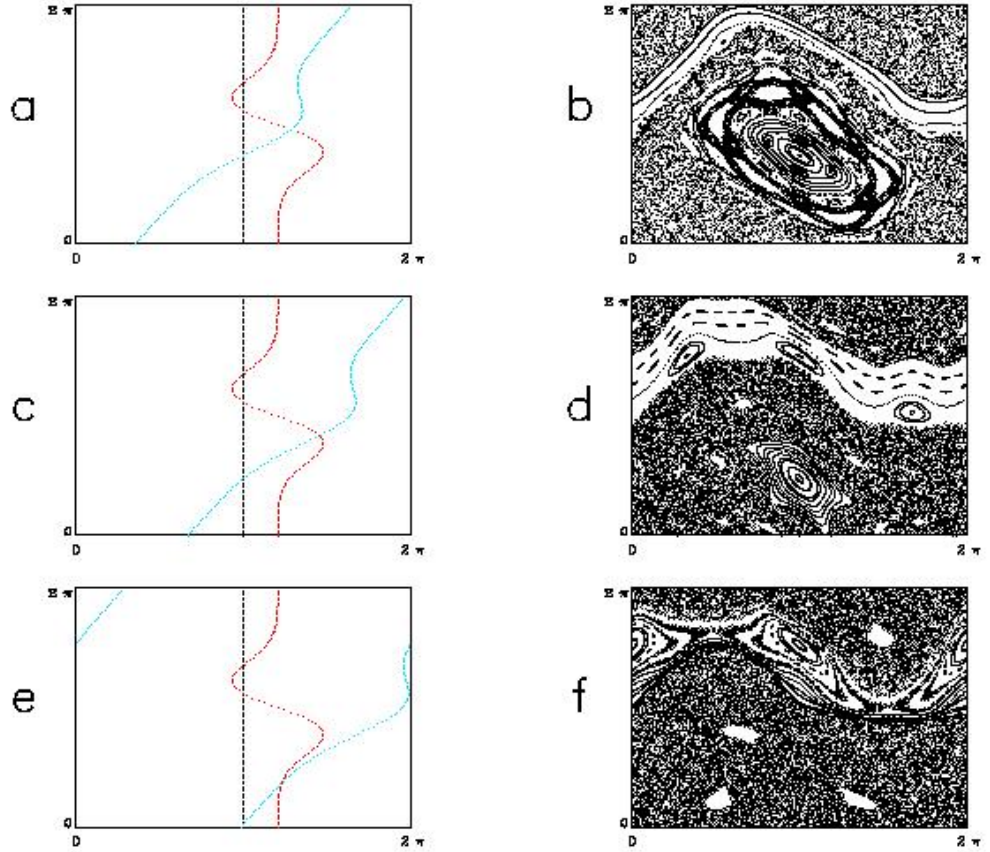


Figure 1: (b), (d) and (f) show Poincaré sections for the map defined by (1) and (2). A small number of points in the (x, y) plane are used as initial conditions for the map and successive iterations are plotted. In chaotic regions the iterates of the map fill out a region of finite area. In barrier regions the iterates of the map fill out a curve. In each case the value of ϵ is chosen to be close to, but less than, the threshold for the 'last barrier' (to transport in the y direction) to disappear. Values of (C, ϵ) are (b) $(0, 1.5)$, (d) $(1, 1.75)$, (f) $(2, 0.5)$. (a), (c), (e) show the corresponding longitudinal displacement (blue) and longitudinal shear (red) profiles. In each of cases (b), (d) and (f) the remaining barrier region is clear as the region where the density of points is low. A rough correspondence is clear between the zero shear locations in (a), (c) and (e) and the remaining barrier regions in (b), (d) and (f). The correspondence is made precise by assigning a longitudinal velocity – defined by the average rate that iterates of the map move in the x -direction – to each of the curves that is mapped out in (b), (d) or (f) (or corresponding curves that could be mapped by starting with different initial conditions). Once a longitudinal velocity has been assigned then it is straightforward to determine the longitudinal shear.

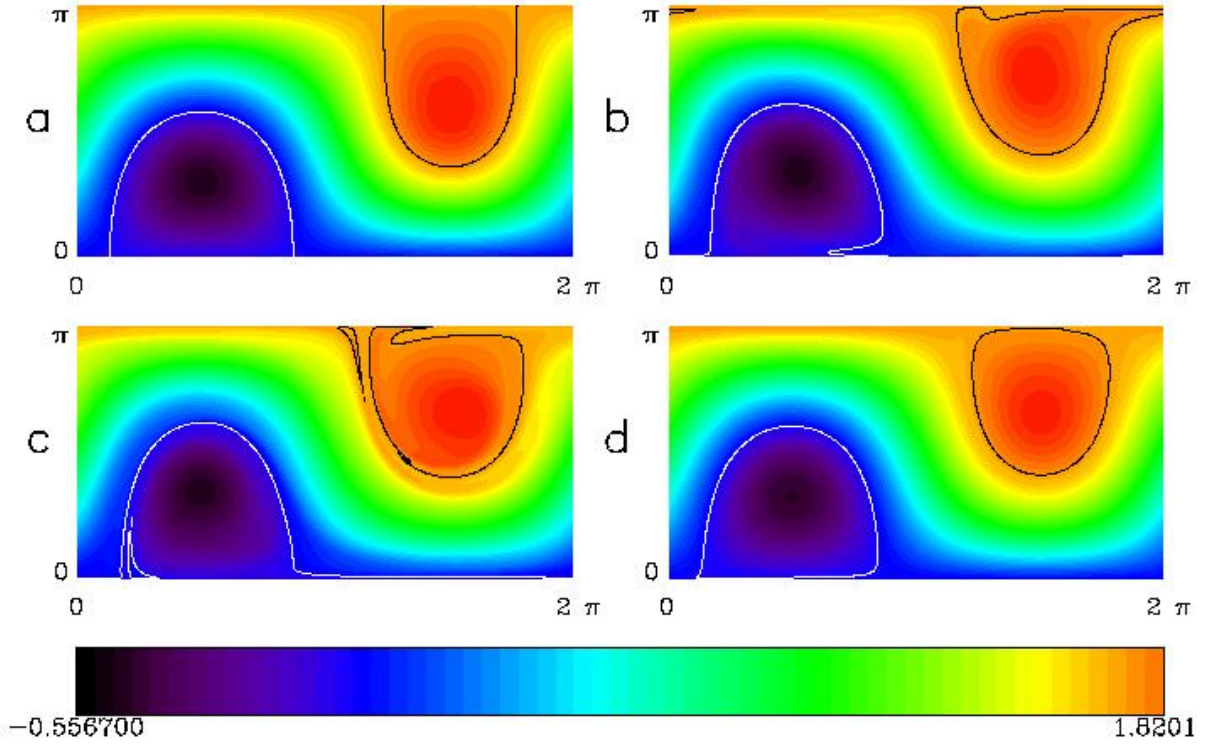


Figure 2: PV field for the case $\epsilon = 0.05$ at times (a) $t = 0$, (b) $t = 0.5\pi/0.3$, (c) $t = \pi/0.3$, (d) $t = 16\pi/0.3$. Note that $2\pi/0.3$ is the period of the imposed topographic forcing in 5. The black and white curves highlight PV contours chosen to coincide with the heteroclinic streamlines (those joining stagnation points) in the initial flow.

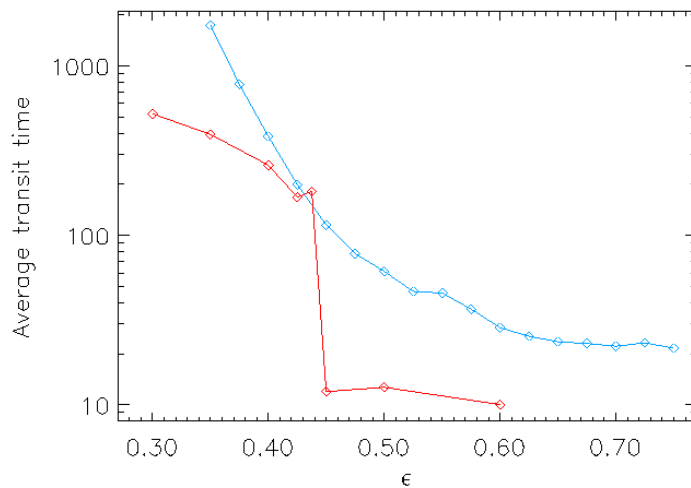


Figure 3: Average transit times to cross the central transport barrier as a function of ϵ in the kinematic model (blue) and the dynamically consistent model (red). See text for discussion.

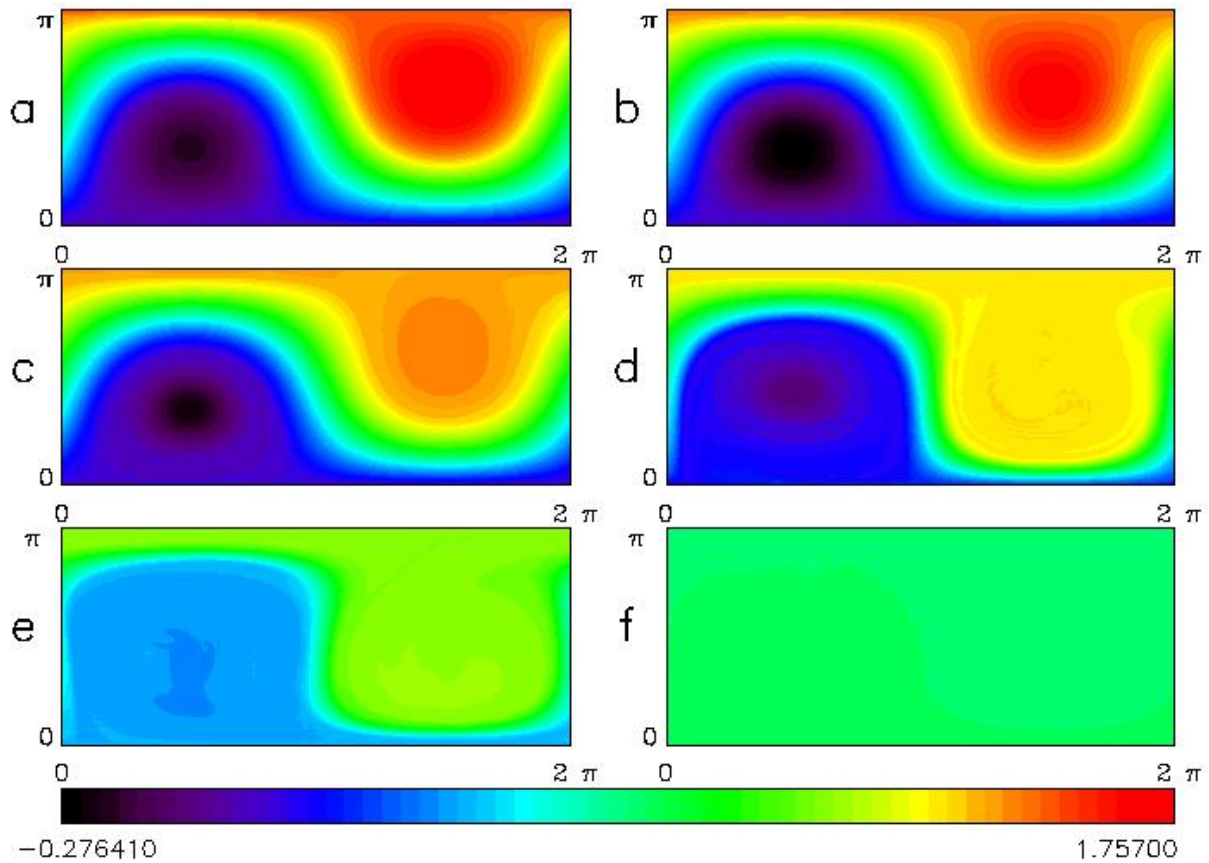


Figure 4: PV field at times $t = 200\pi/0.3$ ($2\pi/0.3$ is the period of the imposed topographic forcing in 5) for (a) $\epsilon = 0$, (b) $\epsilon = 0.05$, (c) $\epsilon = 0.1$, (d) $\epsilon = 0.3$, (e) $\epsilon = 0.4$, (f) $\epsilon = 0.5$. Note that for $\epsilon = 0.5$ the central barrier breaks and the PV therefore essentially homogenises over the domain.

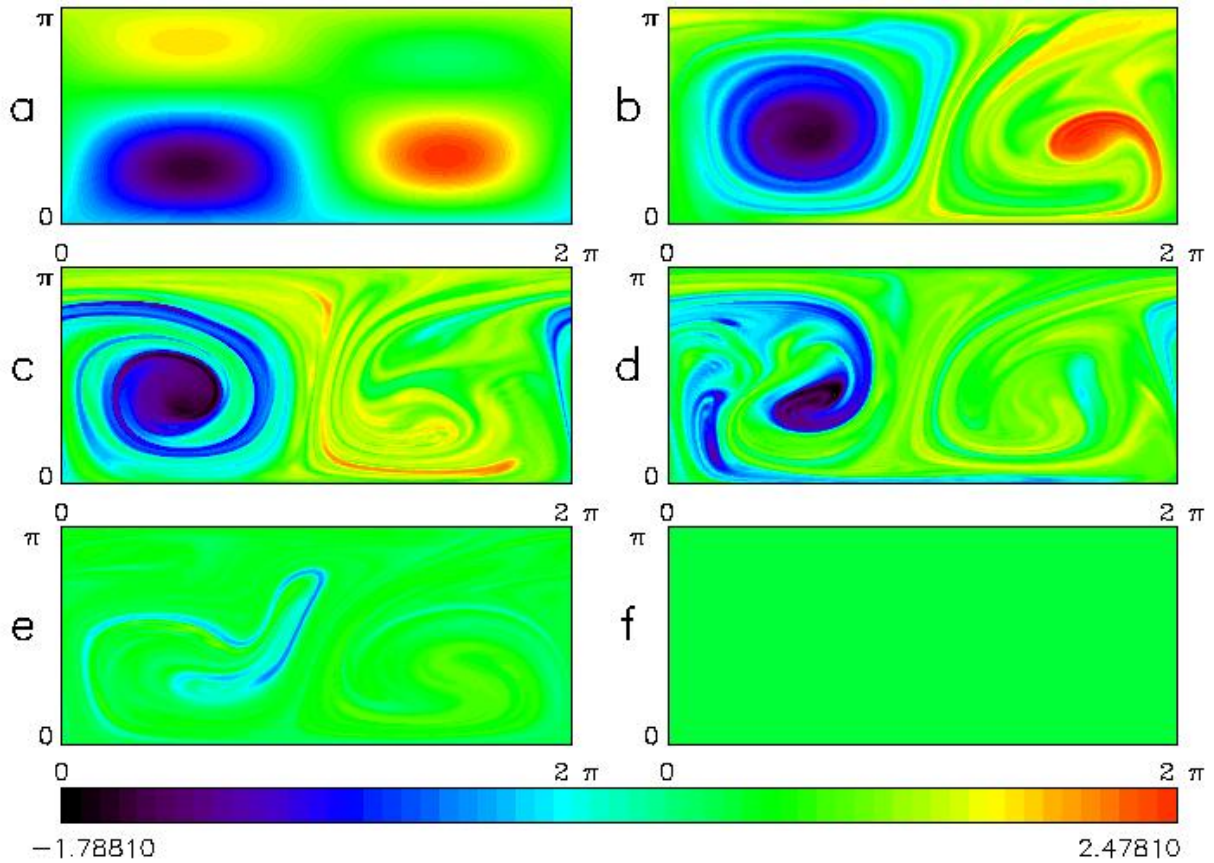


Figure 5: PV field for the case $\epsilon = 0.5$ at times (a) $t = 0$, (b) $t = 2\pi/0.3$, (c) $t = 4\pi/0.3$, (d) $t = 8\pi/0.3$, (e) $t = 16\pi/0.3$, (f) $t = 20\pi/0.3$. Note that $2\pi/0.3$ is the period of the imposed forcing in 5.

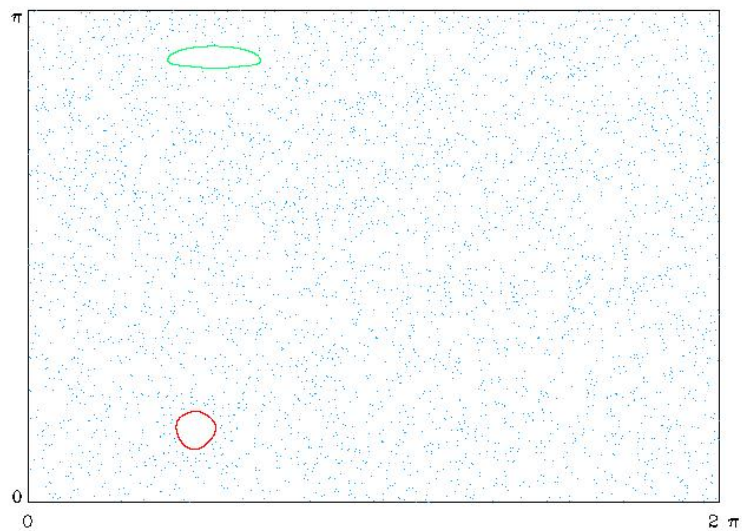


Figure 6: Poincaré section arising from the flow defined by (6) and (5), generated by three initial conditions, two of which lie on barriers and third of which maps out the large chaotic mixing region that covers most of the domain.

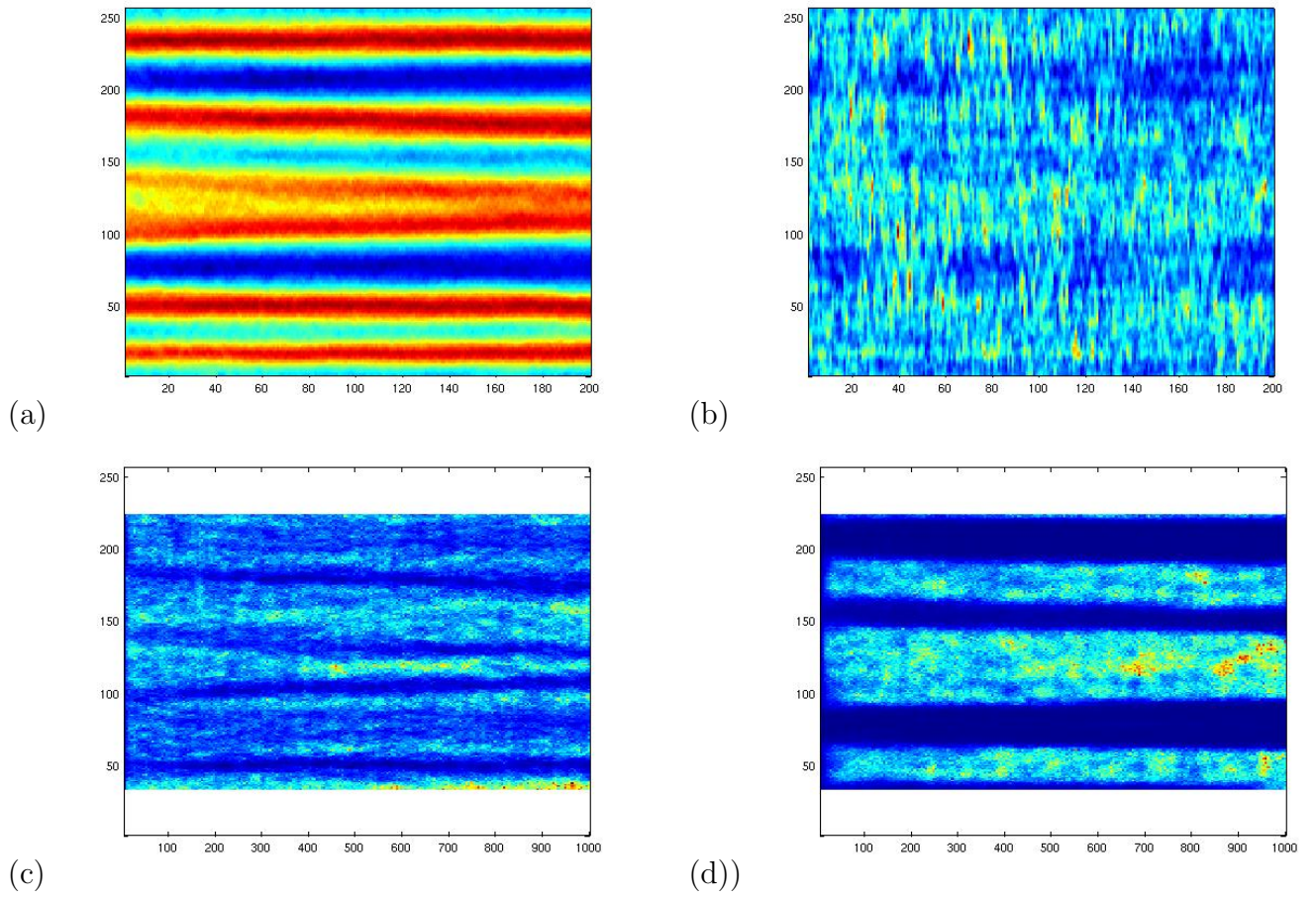


Figure 7: (a) \bar{u} as function of y and t , (b) $\overline{v^2}$ as function of y and t , (c) κ_{eff} calculated from tracer advected with full velocity field, (d) κ_{eff} calculated from tracer advected with \bar{u} removed.